Structural, magnetic, electrical and thermal transport properties in two-dimensional perovskite $Sr_{1.05}Ln_{0.95}CoO_4$ (Ln = La, Ce and Nd) compounds

2008 J. Phys. D: Appl. Phys. 41 215009

(http://iopscience.iop.org/0022-3727/41/21/215009)

IOP PUBLISHING JOURNAL OF PHYSICS D: APPLIED PHYSICS

J. Phys. D: Appl. Phys. **41** (2008) 215009 (6pp) doi:10.1088/0022-3727/41/21/215009

Structural, magnetic, electrical and thermal transport properties in two-dimensional perovskite $Sr_{1.05}Ln_{0.95}CoO_4$ (Ln = La, Ce and Nd) compounds

R Ang[1], **Y P Sun, X B Zhu and W H Song**

Key Laboratory of Materials Physics, Institute of Solid State Physics, and Hefei High Magnetic Field Laboratory, Chinese Academy of Sciences, Hefei 230031, People's Republic of China

E-mail: rang@issp.ac.cn

Received 28 July 2008, in final form 12 September 2008
Published 16 October 2008
Online at stacks.iop.org/JPhysD/41/215009

Abstract

The structural, magnetic, electrical and thermal transport properties have been investigated in two-dimensional layered perovskite $Sr_{1.05}Ln_{0.95}CoO_4$ (Ln = La, Ce and Nd) compounds. The variations of Jahn–Teller distortion of the CoO_6 octahedron and the effective magnetic moment indicate that the induced holes are mostly accommodated in the t_{2g} orbital states keeping the intermediate-spin configuration. The detailed comparison of temperature dependence of magnetization, resistivity, thermoelectric power and thermal conductivity suggests that the tolerance factor t plays a very crucial role in the transport behaviours. With decreasing A-site rare earth ionic radius $r^{3+}_{\rm Ln}$, the tolerance factor t decreases and the distortion of CoO_6 octahedron enhances, which leads to the increased bending of the Co–O–Co bond, the narrowing of the bandwidth and the decrease in the mobility of e_g electrons. In addition, from the viewpoint of application, the huge Seebeck coefficients (>600 μV K^{-1}) indicate that the present layered cobaltites can be good candidates for thermoelectric materials.

1. Introduction

Currently, spintronics has been receiving considerable attention leading to rapid development, because of the unusual coupling among the charge, spin, orbit and lattice degrees of freedom, which are essential for the emergence of complex electronic phenomenon. In particular, the two-dimensional (2D) layered Sr_2CoO_4 compound with a K_2NiF_4-type structure is confirmed to have ferromagnetism (FM) with the highest Curie temperature (T_C = 250 K) [1, 2]. Moritomo *et al* have investigated the low-doped system of $La_{2-x}Sr_xCoO_4$ ($0.4 \leqslant x < 1$) with a mixed valence of Co^{2+} and Co^{3+} ions and proposed a spin-state transition of the Co^{3+} ion from the high-spin (HS) state to the intermediate-spin (IS) state [3]. Further, Chichev *et al* have studied the high-doped system of $La_{2-x}Sr_xCoO_4$ ($1 < x \leqslant 1.4$) with a mixed Co^{3+}/Co^{4+} valency [4]. The IS ground state for $SrLaCoO_4$ is also supported by the optical conductivity spectra. Two broad bands are observed around 2 and 3.5 eV [5, 6]. Wang *et al* have reported that for the $Sr_{2-y}(Y, Gd)_yCoO_4$ ($0 \leqslant y \leqslant 1$) system the spin states for the Co^{3+} and Co^{4+} ions are both IS states at least in the higher temperature range. The observation of enhanced magnetoresistance suggests their potential applications in spintronics [2, 7]. The study of neutron diffraction for the $Sr_{1.4}La_{0.6}CoO_4$ and $SrPrCoO_4$ systems indicates that La and Pr dominate on the Sr-site and yields information on the FM ordering [4, 8]. The purpose of this paper is to understand the magnetic, electrical and thermal transport properties of rare earth element-doped $Sr_{1.05}Ln_{0.95}CoO_4$(Ln = La, Ce and Nd). From the viewpoint of the comparison between different rare earth ionic radii Ln^{3+}, the structural study of the

[1] Author to whom any correspondence should be addressed.

tolerance factor t is very important due to its dominant role in determining the physical properties. It is worth noting that the remarkable thermoelectric power (>600 μV K^{-1}) indicates that the present layered cobaltites may be good candidates for thermoelectric materials. In the previous studied $SrLnCoO_4$ (Ln = La, Ce, Pr, Nd, Eu, Gd and Tb) system, the Co valence is only +3. The ground state shows paramagnetic (PM) behaviour [9]. However, for the present $Sr_{1.05}Ln_{0.95}CoO_4$ system, the Co valence is the mixed state of Co^{3+}/Co^{4+}. We want to know whether the mixed valence of Co ions can influence the physical properties in the $Sr_{1.05}Ln_{0.95}CoO_4$ system.

2. Experimental details

A series of ceramic samples of $Sr_{1.05}Ln_{0.95}CoO_4$ (Ln = La, Ce, and Nd) are synthesized by a conventional solid-state reaction method. Appropriate proportions of high purity Ln_2O_3, $SrCO_3$ and Co_3O_4 powders are thoroughly mixed according to the desired stoichiometry. In order to get relatively homogeneous samples, all the samples are annealed in oxygen circumstance at 800 °C for 12 h. X-ray diffraction (XRD) patterns of the powder samples are obtained on a Philips diffractometer with Cu K_α radiation at room temperature. The XRD pattern reveals that all the samples are in a single phase. It is found that all samples have a tetragonal structure with the space group *I4/mmm* similar to that of the undoped Sr_2CoO_4 system [1, 2]. Every sample is performed by energy dispersive spectroscopy (EDS) analysis. The magnetic measurements are performed on a Quantum Design Physical Property Measurement System (PPMS) ($1.8\,K \leqslant T \leqslant 400\,K$, $0\,T \leqslant H \leqslant 9\,T$). The temperature dependence of resistivity $\rho(T)$, thermoelectric power $S(T)$ and thermal conductivity $\kappa(T)$ is measured by the standard four-probe method in the PPMS.

The oxygen content of the sample is determined by a redox (oxidation–reduction) titration. The detailed method to determine the oxygen content of the sample has been reported elsewhere [10]. For the samples of $Sr_{1.05}Ln_{0.95}CoO_{4+\delta}$, only slightly excess oxygen $\delta < 0.01$ is observed. The EDS analysis indicates that the nominal value and the analysed one are the same for each sample. Thus the stoichiometric $Sr_{1.05}Ln_{0.95}CoO_4$ can represent our samples, where slightly excess oxygen is ignored.

3. Results and discussion

Figure 1 shows a schematic representation of the structure of $Sr_{1.05}Ln_{0.95}CoO_4$. The structure is 2D and can be described as the CoO_2 planes separated by double rock-salt layers of SrO, in which the Co ions are in a usually distorted octahedral environment while the Sr^{2+}/Ln^{3+} cations are 9-coordinated. The structure refinements are carried out by the standard Rietveld technique [11]. The refined lattice parameters as a function of different A-site rare earth ionic radii are shown in figure 2. It can be seen from figure 2(a) that both a and c decrease gradually with decreasing A-site ionic radius r^{3+}_{Ln} (i.e. $r^{3+}_{La} = 1.216$ Å $> r^{3+}_{Ce} = 1.196$ Å $> r^{3+}_{Nd} = 1.163$ Å). In addition, the cell volume V decreases as the size of r^{3+}_{Ln} diminishes (figure 2(b)). The decrease in the lattice parameters is in agreement with the fact that the sizes of Ln^{3+} ions are smaller than that of the Sr^{2+} ion ($r^{2+}_{Sr} = 1.310$ Å).

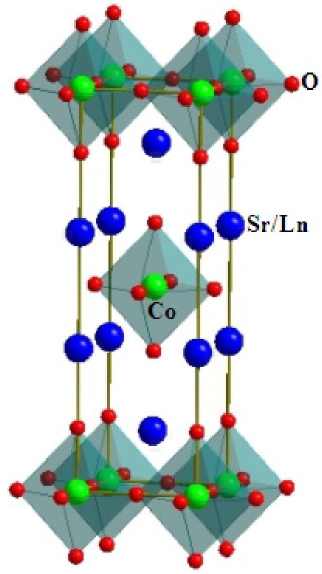

Figure 1. Schematic representation of the structure of $Sr_{1.05}Ln_{0.95}CoO_4$ (Ln = La, Ce, Nd).
(This figure is in colour only in the electronic version)

In figure 1, the Co ions are in a distorted octahedral site within the perovskite blocks, so that there are two different Co–O bond lengths: a longer Co–O(1) along the $c$axis and a shorter Co–O(2) in the ab plane. As shown in figure 2(c), both Co–O(1) and Co–O(2) distances monotonically decrease as the size of r^{3+}_{Ln} gets smaller. Refinement results indicate that for the $Sr_{1.05}La_{0.95}CoO_4$ sample the in-plane Co–O(2) bond length (1.902 Å) and the Co–O(1) bond distance along the c axis (2.034 Å) are both longer than those of $Sr_{1.05}Nd_{0.95}CoO_4$ (ab plane: 1.885 Å, c axis: 2.020 Å). The extent of the distortion from the CoO_6 octahedral coordination can be estimated from the difference Δd between Co–O(1) and Co–O(2) bond lengths (figure 2(d)). Interestingly, the value of the distortion parameter Δd increases with decreasing r^{3+}_{Ln}. For the $Sr_{1.05}Nd_{0.95}CoO_4$ sample, Δd is 0.1348 Å, which indicates that there is a stronger distortion in the CoO_6 octahedron compared with that of $Sr_{1.05}La_{0.95}CoO_4$ ($\Delta d = 0.1319$ Å). Actually, the distortion of the CoO_6 octahedron, which can also be reflected by the ratio of the Co–O(1) bond length $d_{Co-O(1)}$ to the Co–O(2) one $d_{Co-O(2)}$. The ratio $d_{M-O(1)}/d_{M-O(2)}$ is approximately 1.20 (M = Mn, e^1_g) for the e_g-orbital-driven Jahn–Teller (JT) distortion in $LaSrMnO_4$ [12] and 1.02 (M = Ru, t^4_{2g}) for the t_{2g}-orbital-driven one in Ca_2RuO_4 [13]. Thus, the bond length ratio from $Sr_{1.05}La_{0.95}CoO_4$ (1.0693) to $Sr_{1.05}Nd_{0.95}CoO_4$ (1.0715) indicates the situation where the e_g states of the IS configuration are not only fully occupied by $3d_{3z^2-r^2}$ orbitals but also partially by $3d_{x^2-y^2}$ states. In the present layered system, the IS configuration appears to be further favoured rather than the HS or low-spin (LS) one due to the ligand field splitting of e_g states and the distortion of the CoO_6 octahedron. The gain of kinetic energy of the e_g electron also contributes to the stabilization of the IS ground state relative to the LS one. The gradual increase in $d_{Co-O(1)}/d_{Co-O(2)}$ with decreasing r^{3+}_{Ln}

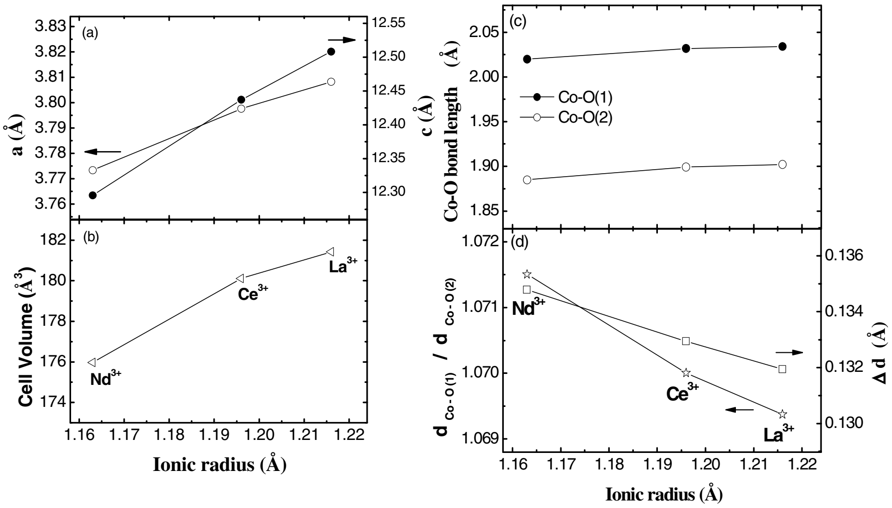

Figure 2. (*a*) and (*b*) Variations of lattice parameters of $Sr_{1.05}Ln_{0.95}CoO_4$. (*c*) and (*d*) The ionic radius dependence of the Co–O (1) and Co–O (2) bond lengths.

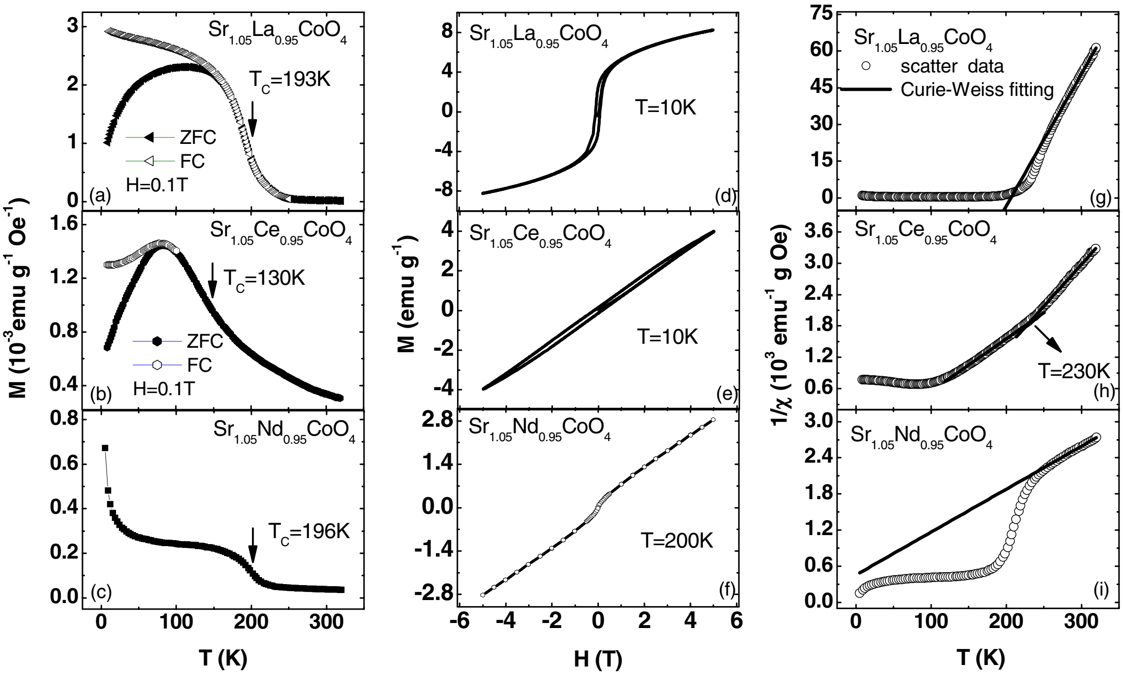

Figure 3. (*a*)–(*c*) The temperature dependence of magnetization $M(T)$. (*d*)–(*f*) The field dependence of magnetization $M(H)$. (*g*)–(*i*) The temperature dependence of the inverse susceptibility $\chi^{-1}(T)$. The solid lines stand for the Curie–Weiss fitting for $Sr_{1.05}La_{0.95}CoO_4$, $Sr_{1.05}Ce_{0.95}CoO_4$ and $Sr_{1.05}Nd_{0.95}CoO_4$, respectively.

implies that the induced holes are mainly accommodated in the t_{2g} orbital states [13]. The $Sr_{1.05}Nd_{0.95}CoO_4$ sample has more JT distortions compared with that of other samples.

The temperature dependence of magnetization $M(T)$ measured in an applied field of $H = 0.1$ T for all the samples is shown in figures 3(*a*)–(*c*), respectively. For the La-doped sample, the Curie temperature T_C (defined as the one corresponding to the peak of dM/dT in the M versus T curve) is 193 K. It is clear that the zero field cooling (ZFC) curve does not coincide with the field cooling (FC) curve below a freezing temperature. The discrepancy between ZFC and FC magnetization is a characteristic of glass. The induced FM can originate from the FM interaction between Co^{3+} and Co^{4+} ions. The substitution of La^{3+} for Sr^{2+} induces a large variation in the Co valence and consequent FM interaction in the mixed-valent state of Co^{3+}/Co^{4+}. The Ce-doped sample also shows behaviour similar to the La-doped one as shown in figure 3(*b*). It is worth noting that for the Nd-doped sample, there also exists a FM transition and the transition temperature is 196 K. However, PM behaviour is exhibited at low temperatures (figure 3(*c*)). The magnitude of magnetization decreases with decreasing r_{Ln}^{3+}. In addition, figures 3(*d*)–(*f*) show the field dependence of magnetization $M(H)$ from -5 T to 5 T at $T = 10$ K and 200 K for La-, Ce- and Nd-doped samples, respectively. The magnetization M increases continuously without saturation up to 5 T, revealing a superposition of both

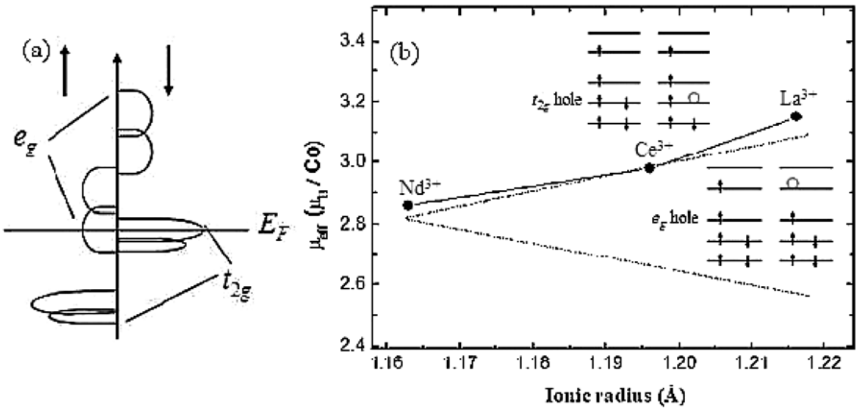

Figure 4. (*a*) Schematic representation of DOS for up-spin and down-spin Co-e_g and t_{2g} bands in conducting layered $Sr_{1.05}Ln_{0.95}CoO_4$ (Ln = La, Ce, Nd). (*b*) The effective moment μ_{eff} per Co site for $Sr_{1.05}Ln_{0.95}CoO_4$. The broken lines are calculated for the case that all doped holes go into t_{2g} or e_g states, respectively.

FM and antiferromagnetic (AFM) components. It can be found that the magnetic hysteresis and the coercive forces H_C of $Sr_{1.05}$(La, Ce)$_{0.95}CoO_4$ samples are larger than that of the $Sr_{1.05}Nd_{0.95}CoO_4$ sample. Such a larger H_C is due to the larger blocking of the domain wall motion [14] in the $Sr_{1.05}$(La, Ce)$_{0.95}CoO_4$ samples. It is noted that we have also measured the $M(H)$ curve at 10 K for the $Sr_{1.05}Nd_{0.95}CoO_4$ sample. However, it only behaves like a straight line. Such a result confirms the PM background at low temperatures for the Nd-doped sample. Additionally, no bifurcation between FC and ZFC is observed for the Nd-doped sample. That is to say, the PM behaviour at low temperatures for the Nd-doped sample should originate from the PM contribution of Nd^{3+}.

In order to study the magnetic interaction further, $1/\chi$ versus T curves are plotted in figures 3(*g*)–(*i*). For the $Sr_{1.05}La_{0.95}CoO_4$ sample, the data in the PM region are fitted according to the Curie–Weiss law, $\chi = C/(T - \Theta)$, where C is the Curie constant and Θ is the Weiss temperature. The scatters are the experimental data and the solid line is the fitted one (figure 3(*g*)). The fitted value of Θ is 206 K. The positive Θ indicates the presence of FM interaction. It is found that the Curie–Weiss law is not satisfactory with the experimental curve in the temperature range of 210–246 K. The deviation of the inverse susceptibility, $1/\chi$, from the high temperature straight line corresponding to noninteraction magnetic moments marks the onset of the magnetic interaction between magnetic moments [15]. For the La-doped sample, below 246 K the PM state appears to be dominated by local FM fluctuations that are presumably mediated by Co^{3+}/Co^{4+} FM interactions induced by e_g electron hopping. Namely, there exist magnetic clusters in the PM region. For the Nd-doped sample, it is very clear about the deviation as well as that of La-doped sample (figure 3(*i*)). Nevertheless, the $Sr_{1.05}Ce_{0.95}CoO_4$ sample shows an abnormal behaviour in the slope of the $\chi^{-1}(T)$ curve around 230 K (figure 3(*h*)). The fitting in the PM region also obeys the Curie–Weiss law. Above 230 K, the fitted value of Θ is 114 K. Below 230 K, the fitted value of Θ is 45 K. The crossover near 230 K can be related to the spin-state transition of Co ions.

Figure 4(*a*) shows a schematic representation of density of states (DOS) for the $Sr_{1.05}Ln_{0.95}CoO_4$ sample. The Co-3d electrons form the localized t_{2g} band. The remaining electrons occupy the conducting e_g band which is energetically higher than the t_{2g} band in the crystal field. The e_g band further splits due to JT distortion into two sub-bands, which are separated by the JT splitting energy. Meanwhile, the JT distortion also causes a splitting of the t_{2g} band. Both the splitting e_g sub-bands and the t_{2g} sub-bands will cross due to the weak JT splitting energy. Moreover, Hund's rule coupling removes the spin degeneracy in the FM state. The resulting separation of the spin-up ($e_g \uparrow, t_{2g} \uparrow$) and spin-down ($e_g \downarrow, t_{2g} \downarrow$) is denoted, respectively. The $t_{2g} \downarrow$ is energetically lower than $e_g \uparrow$. Both the $e_g \uparrow$ and $t_{2g} \downarrow$ states are partially occupied, which comprise the quasimetallic bands in the layered $Sr_{1.05}Ln_{0.95}CoO_4$. The change in the nature of induced holes is manifested by the effective magnetic moment μ_{eff} (per Co ion) derived from the Curie–Weiss plot. The upper and lower broken lines in figure 4(*b*) represent the calculated values from $\mu_{eff} = 2\sqrt{S(S+1)}$ for the t_{2g}-hole ($e_g^1 t_{2g}^{5-x}$) and e_g-hole ($e_g^{1-x} t_{2g}^5$), respectively. As a result, the observed variation of μ_{eff} is well in accord with the t_{2g}-hole picture.

Obviously, the different behaviours of magnetization for all the samples depend on the ionic size of Ln^{3+}. As we know, for $La_{1-x}A_xBO_3$ (A = Ca, Sr and Ba; B = Mn and Co) manganites and cobaltites [16, 17], it is argued that the magnetization and the transition temperature are mainly determined by a global distortion arising from the deviation of the structure from the cubic perovskite. This distortion can be described by the deviation of the tolerance factor $t = (\langle r_A \rangle + r_O)/[\sqrt{2}(r_B + r_O)]$ from $t = 1$ where r_B and r_O denote the ionic radii of the B and O ions and $\langle r_A \rangle$ is the average radius of the ions on the A-site. For the present $Sr_{1.05}Ln_{0.95}CoO_4$, the tolerance factor t can play an important role in determining the behaviour of magnetization. Directly speaking, with decreasing r_{Ln}^{3+}, the tolerance factor t decreases and the distortion of CoO_6 octahedron becomes stronger, which leads to the narrowing of the bandwidth. Therefore, the magnitude of magnetization of the $Sr_{1.05}Nd_{0.95}CoO_4$ sample does not exceed those of other samples.

Figure 5(*a*) shows the temperature dependence of resistivity $\rho(T)$. It indicates that ρ increases with decreasing

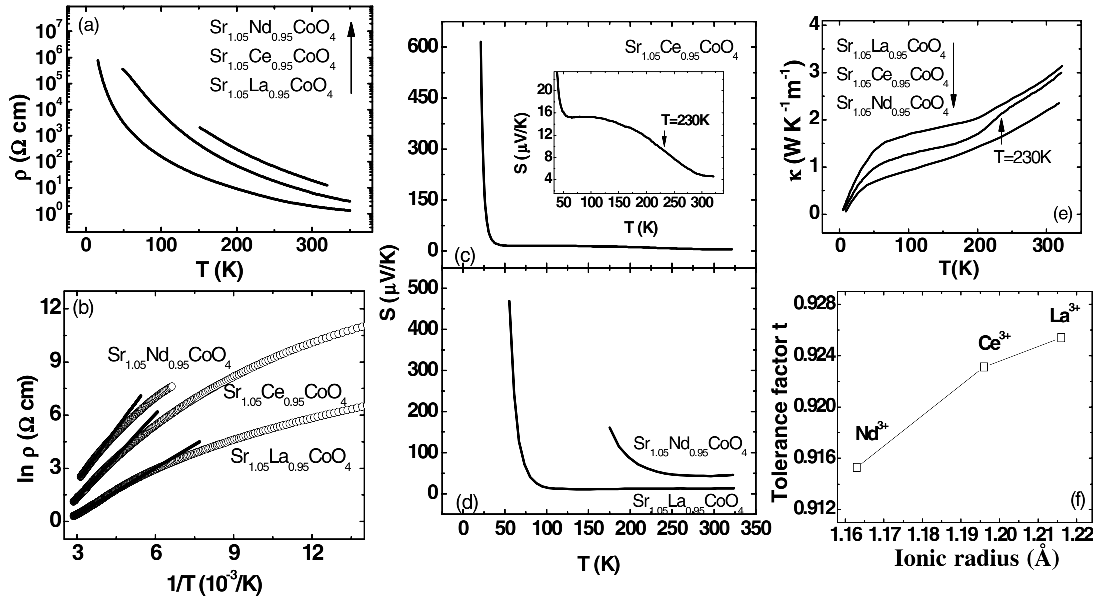

Figure 5. (*a*) The temperature dependence of resistivity $\rho(T)$. (*b*) The plot of $\ln\rho$ against T^{-1}. The solid lines stand for thermally activated conduction fitting. (*c*) and (*d*) The temperature dependence of the Seebeck coefficient $S(T)$. (*e*) The temperature dependence of thermal conductivity $\kappa(T)$. (*f*) The ionic radius dependence of the tolerance factor t.

r_{Ln}^{3+} and all samples have semiconducting behaviour in the whole measured temperature range. The magnitude of ρ at low temperatures is very large ($>10^5\,\Omega$ cm). Comparatively, the 3D perovskite $La_{0.5}Sr_{0.5}CoO_3$ is a good conductor with $\rho < 10^{-4}\,\Omega$ cm [18]. The increase in ρ with decreasing r_{Ln}^{3+} is attributed to the decreased tolerance factor t and the weaker mobility of e_g electrons. The high temperature $\rho(T)$ data can be fitted by the thermally activated conduction law [19], $\rho(T) = \rho_0 \exp(E_a/k_B T)$, where E_a is the activation energy. The plot of $\ln\rho$ against T^{-1} is plotted in figure 5(*b*). The value of E_a increases from $Sr_{1.05}La_{0.95}CoO_4$ (76 meV) to $Sr_{1.05}Nd_{0.95}CoO_4$ (173 meV) with decreasing r_{Ln}^{3+}.

Compared with the 3D cobaltite system, e_g electrons of the present 2D system are expected to show different behaviours. In the 3D system, the σ^* band is formed from hybridization of Co-$3d_{3z^2-r^2}$ and O-2p orbitals along the c axis as well as from Co-$3d_{x^2-y^2}$ and O-2p orbitals along the *ab* plane. However, in the layered system, the σ^* band would be mainly composed of the $33d_{x^2-y^2}$ and O-2p orbitals with a less contribution of the $3d_{3z^2-r^2}$ orbitals because of the 2D confinement of the Co–O–Co network. Due to the tetragonal symmetry of the CoO_6 octahedron, both t_{2g} and e_g states are further split into two levels. If the electrons in orbitals other than $3d_{x^2-y^2}$ tend to be localized, a semiconducting nature is expected for the 2D system with the IS state. This may explain the higher ρ of the present 2D layered system compared with the 3D perovskite system.

Figures 5(*c*) and (*d*) show the temperature dependence of the Seebeck coefficient $S(T)$. All the samples have semiconducting-like behaviour. For the $Sr_{1.05}Ce_{0.95}CoO_4$ sample (figure 5(*c*)), a transition near 230 K is observed, which is the same as that of magnetization. Namely, the spin-state transition of Co ions can occur. It is surprising that for all the samples the magnitude of S is very large. The values of $S = 615\,\mu\mathrm{V\,K^{-1}}$ at 21 K and $S = 470\,\mu\mathrm{V\,K^{-1}}$ at 55 K for $Sr_{1.05}Ce_{0.95}CoO_4$ and $Sr_{1.05}La_{0.95}CoO_4$ are obtained, respectively. Especially, the magnitude of $S_{300\,\mathrm{K}}$ at room temperature increases with decreasing r_{Ln}^{3+}, which is attributed to the enhanced spin entropy due to the weakened magnetic interaction caused by the narrowing of the bandwidth.

The temperature dependence of thermal conductivity $\kappa(T)$ is shown in figure 5(*e*). According to the Wiedemann–Franz law, the measured κ_{tot} comes mostly from the contribution of the phononic κ_{ph} due to the ignored electronic κ_e. For the $Sr_{1.05}La_{0.95}CoO_4$ sample, κ increases rapidly above 200 K with increasing temperature. For the sample with $Sr_{1.05}Ce_{0.95}CoO_4$, κ decreases and a spin state transition of Co ions is still observed near 230 K. κ decreases in the whole temperature range with decreasing r_{Ln}^{3+}. Furthermore, the rather low κ values ($<4\,\mathrm{W\,K^{-1}\,m^{-1}}$), indicating a phonon mean free path with the order of a lattice spacing, are considered to correlate with the distortion of the $Co^{3+}O_6$ octahedron with an IS state. As is well known, the $Co^{3+}O_6$ lattice distortion due to the Co^{3+} ion with the IS state can scatter the phonons [20]. With decreasing r_{Ln}^{3+}, the tolerance factor$t$ reduces and the distortion in CoO_6 octahedron enhances contributing to the decrease in κ.

Based on the above results, it can be concluded that the tolerance factor t is the dominating factor that strongly influences the structural, magnetic, electrical and thermal transport properties in the 2D layered perovskite $Sr_{1.05}Ln_{0.95}CoO_4$ system. The standard ionic radii for different elements are used to calculate t. The tolerance factor$t$ as a function of the ionic radius r_{Ln}^{3+} is plotted in figure 5(*f*). It is found that with the decrease in r_{Ln}^{3+}, t decreases due to the substitution of smaller Ln^{3+} ions for a larger Sr^{2+} ion. The CoO_6 octahedral distortion increases and the bending of the Co–O–Co bond becomes obvious. Finally, the bandwidth gets narrower and the mobility of e_g electrons reduces. Hence the $Sr_{1.05}Nd_{0.95}CoO_4$ sample with the smaller A-site ionic radius exhibits lower M, higher ρ, higher S and lower κ.

4. Conclusions

In summary, we have investigated the structural, magnetic, electrical and thermal properties for the layered perovskite $Sr_{1.05}Ln_{0.95}CoO_4$ (Ln = La, Ce and Nd) with the K_2NiF_4-type structure. The variations of JT distortion of the CoO_6 octahedron and μ_{eff} indicate that the induced holes mostly enter the t_{2g} orbital states while retaining the IS configuration. The detailed comparison of the temperature dependence of $M(T)$, $\rho(T)$, $S(T)$ and $\kappa(T)$ suggests that t dominates the transport behaviours. The decrease of t with decreasing r_{Ln}^{3+} and the stronger distortions of CoO_6 octahedron, which brings on the enhanced bending of Co–O–Co bond, the narrowing of the bandwidth and the decrease of the mobility of e_g electrons.

Acknowledgment

This work was supported by the National Key Basic Research under contract No 2007CB925002 and the National Nature Science Foundation of China under contract No 10774146, No 50672099, 50701042 and Director's Fund of Hefei Institutes of Physical Science, Chinese Academy of Sciences.

References

[1] Matsuno J, Okimoto Y, Fang Z, Yu X Z, Matsui Y, Nagaosa N, Kawasaki M and Tokura Y 2004 *Phys. Rev. Lett.* **93** 167202
[2] Wang X L and Takayama-Muromachi E 2005 *Phys. Rev.* B **72** 064401
[3] Moritomo Y, Higashi K, Matsuda K and Nakamura A 1997 *Phys. Rev.* B **55** R14725
[4] Chichev A V *et al* 2006 *Phys. Rev.* B **74** 134414
[5] Uchida S, Eisaki H and Tajima S 1993 *Physica* B **186–188** 975
[6] Moritomo Y, Arima T and Tokura Y 1995 *J. Phys. Soc. Japan* **64** 4117
[7] Wang X L, Takayama-Muromachi E, Dou S X and Cheng Z X 2007 *Appl. Phys. Lett.* **91** 062501
[8] Bowman A, Claridge J B and Rosseinsky M J 2006 *Chem. Mater.* **18** 3046
[9] Ang R, Sun Y P, Luo X, Hao C Y and Song W H 2008 *J. Phys. D: Appl. Phys.* **41** 045404
[10] Yang J, Song W H, Ma Y Q, Zhang R L and Sun Y P 2005 *J. Magn. Magn. Mater.* **285** 417
[11] Wiles D B and Young R A 1981 *J. Appl. Crystallogr.* **14** 149
[12] Herrero-Martín J, García J, Subías G, Blasco J and Sánchez M C 2005 *Phys. Rev.* B **72** 085106
[13] Friedt O, Braden M, AndréG, Adelmann P, Nakatsuji S and Maeno Y 2001 *Phys. Rev.* B **63** 174432
[14] Lu W J, Sun Y P, Ang R, Zhu X B and Song W H 2007 *Phys. Rev.* B **75** 014414
[15] Causa M T *et al* 1998 *Phys. Rev.* B **58** 3233
[16] Hwang H Y, Cheong S W, Radaelli P G, Marezio M and Batlogg B 1995 *Phys. Rev. Lett.* **75** 914
[17] Kriener M, Zobel C, Reichl A, Baier J, Cwik M, Berggold K, Kierspel H, Zabara O, Freimuth A and Lorenz T 2004 *Phys. Rev.* B **69** 094417
[18] Senarfs-Rodriguez M A and Goodenough J B 1995 *J. Solid State Chem.* **118** 323
[19] Mott N F and Davis E A 1971 *Electronic Processes in Non-Crystalline Materials* (Oxford: Clarendon)
[20] Matsukawa M, Narita M, Nishimura T, Yoshizawa M, Apostu M, Suryanarayanan R, Revcolevschi A, Itoh K and Kobayashi N 2003 *Phys. Rev.* B **67** 104433